
HEURISTIC MULTIOBJECTIVE DISCRETE OPTIMIZATION USING RESTRICTED DECISION DIAGRAMS

A PREPRINT

Rahul Patel¹, Elias B. Khalil¹, David Bergman²

¹Department of Mechanical and Industrial Engineering, University of Toronto

²Department of Operations and Information Management, University of Connecticut
rm.patel@mail.utoronto.ca, khalil@mie.utoronto.ca

ABSTRACT

Decision diagrams (DDs) have emerged as a state-of-the-art method for exact multiobjective integer linear programming. When the DD is too large to fit into memory or the decision-maker prefers a fast approximation to the Pareto frontier, the complete DD must be restricted to a subset of its states (or nodes). We introduce new node-selection heuristics for constructing restricted DDs that produce a high-quality approximation of the Pareto frontier. Depending on the structure of the problem, our heuristics are based on either simple rules, machine learning with feature engineering, or end-to-end deep learning. Experiments on multiobjective knapsack, set packing, and traveling salesperson problems show that our approach is highly effective, recovering over 85% of the Pareto frontier while achieving $2.5\times$ speedups over exact DD enumeration on average, with very few non-Pareto solutions. The code is available at <https://github.com/rahulptel/HMORDD>.

Keywords Multiobjective optimization · Decision Diagrams · Machine Learning

1 Introduction

Real-world decision-making rarely involves a single criterion. Instead, one must frequently trade off conflicting goals, such as maximizing profit while minimizing risk, or maximizing service quality while minimizing cost. These scenarios are modeled with *multiobjective optimization* (MOO). Unlike single-objective optimization, where the goal is to find a single optimal solution, the goal in MOO is to identify the *Pareto frontier*—the set of feasible solutions for which no objective can be improved without worsening another. In this work, we focus on *multiobjective integer linear programming* (MOILP), i.e., MOO problems with integer variables and linear constraints and objectives. Just as the framework of integer linear programming is widely used to model single-objective decision-making tasks, its multiobjective counterpart has found various applications in multicriteria decision-making [17, 18].

In recent years, *decision diagrams* (DDs) have emerged as a powerful alternative to traditional enumerative methods. Initially introduced for representing switching circuits [25] and later popularized for formal verification [12], DDs were adapted for discrete optimization problems by compactly encoding their feasible set [6]. A DD is a directed acyclic graph where paths from the root to the terminal node correspond to feasible solutions. Building on this success, recent works have extended DDs to the multiobjective setting [4, 3] and achieved state-of-the-art results for problems amenable to dynamic programming formulations. By representing the solution space compactly, exact DDs often outperform traditional algorithms for problems with 2–10 objectives and hundreds of variables.

The major bottleneck for exact methods such as DDs is that the size of the Pareto frontier can grow exponentially with instance size, making exact enumeration computationally prohibitive and often overwhelming for the decision-maker. In many practical scenarios, a user requires that a high-quality approximation of the frontier be delivered quickly, rather than a delayed exact set. To address this issue, several heuristics have been proposed in the literature [16, 39, 36, 30, 31, 2].

Within the context of DDs, one can *restrict* the diagram to obtain an approximate Pareto frontier. A restricted DD limits the width of the graph (the number of nodes per layer), thereby discarding some feasible solutions to maintain

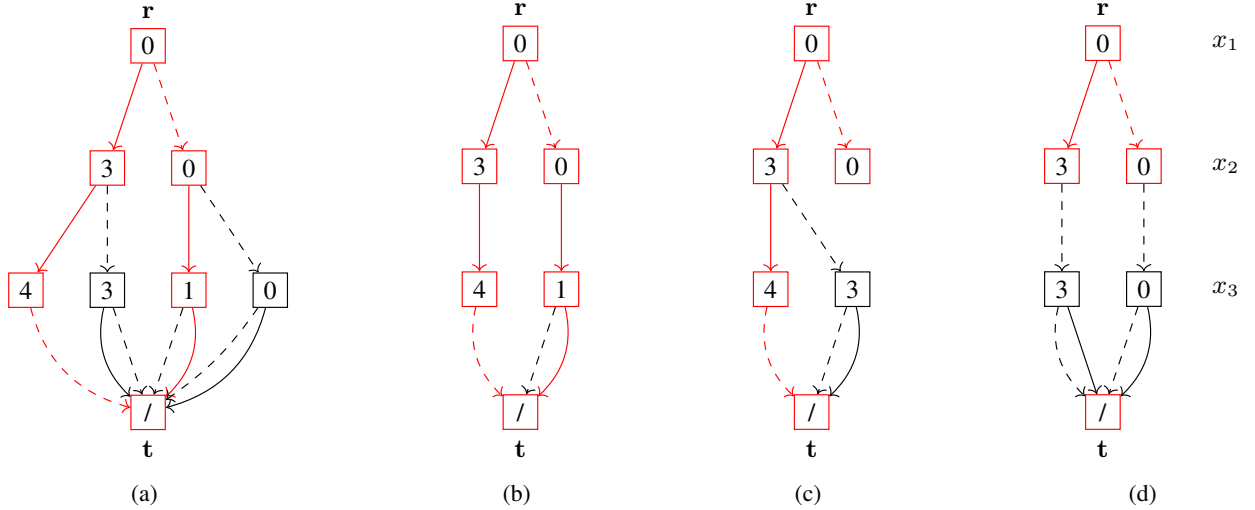


Figure 1: The exact and restricted DDs for Example 1.1. The paths corresponding to the Pareto-optimal solutions $(1, 1, 0)$ and $(0, 1, 1)$, along with their associated Pareto nodes, are highlighted in red. (a) Exact DD. (b) Restricted DD with complete recovery of the Pareto frontier. (c) Restricted DD with partial recovery of the Pareto frontier. (d) Restricted DD with no recovery of the Pareto frontier.

a manageable size. While restricted DDs are widely used to obtain bounds [7, 5, 13, 27] in single-objective problems, their application to multiobjective optimization remains largely unexplored. To the best of our knowledge, this work is the first to address the challenge of constructing a restricted DD that quickly recovers a large fraction of the true Pareto frontier, thereby extending the use of DDs to heuristic MOO.

Illustrative example. Consider the knapsack problem in Example 1.1 and the corresponding exact DD in Figure 1.

Example 1.1 (A bi-objective knapsack problem).

$$\min_{x \in \{0,1\}^3} (x_1 + 10x_2 + 3x_3, 2x_1 + 3x_2 + x_3) \text{ such that } 3x_1 + x_2 + 2x_3 \leq 5.$$

The state in this case, represented by a square node, is equal to the weight of the items selected in the knapsack. We start with an empty knapsack, represented by the root node r with weight 0. From there on, in each layer we decide whether to select an item or not. For example, selecting (not selecting) item x_1 is represented by a solid (dashed) arc from the root node, resulting in a state with a value 3 (or 0). Note that only the red nodes are used by the two Pareto solutions. A restricted DD comprising only of the red nodes preserves the Pareto frontier. Additionally, the red nodes are a small fraction of the total nodes in the DD. Hence, if one can construct a restricted DD with only the red nodes, the Pareto frontier can be recovered quickly.

Table 1 reports the percentage of Pareto nodes observed across three benchmark problem classes—MOSPP, MOKP, and MOTSP—for varying numbers of objectives and decision variables, averaged over ten instances per configuration. Overall, the results indicate that Pareto nodes constitute only a small fraction of the total nodes in a DD.

Empirical justification. This phenomenon is not accidental: in random instances of the multiobjective knapsack problem (MOKP), multiobjective set packing problem (MOSPP), and multiobjective traveling salesperson problem (MOTSP), only a very small fraction of DD nodes (between 1% and 12%) lead to Pareto-optimal solutions, as detailed in Table 1. We refer to these nodes as *Pareto nodes*. If one could identify these nodes in advance and restrict the DD

Table 1: Average percentage of Pareto nodes (rounded) across problem classes and instance sizes (number of objectives and variables), computed over 10 instances.

MOSPP	Pareto Node (%)	MOKP	Pareto Node (%)	MOTSP	Pareto Node (%)
(3, 100)	1	(3, 80)	3	(3, 15)	2
(5, 100)	1	(5, 40)	7	(4, 15)	6
(7, 100)	2	(7, 40)	12		

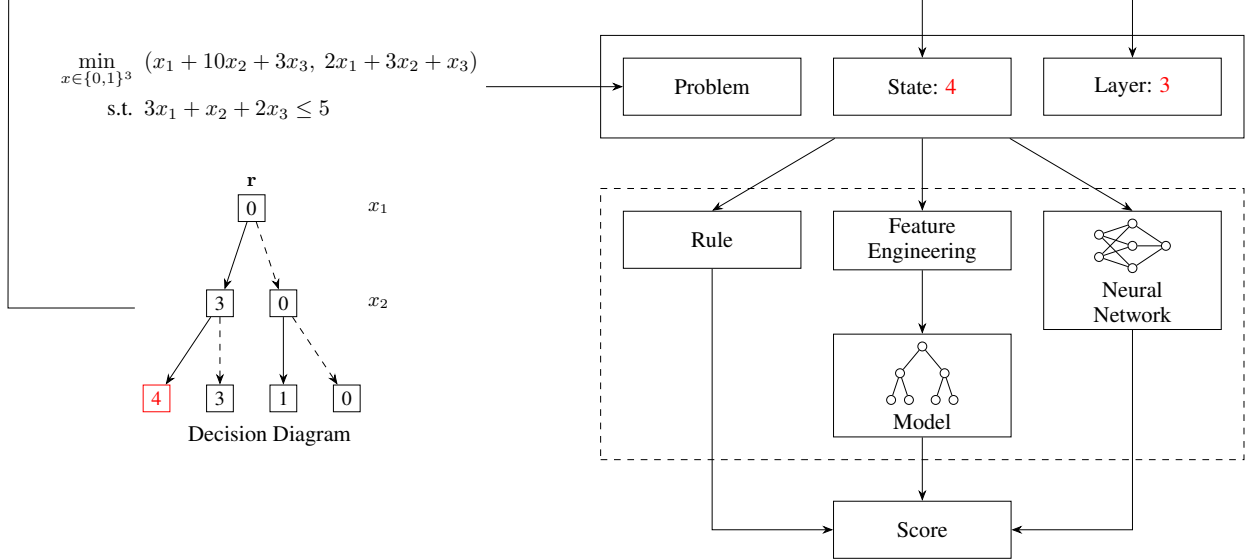


Figure 2: A schematic illustration of the node-selection pipeline in restricted DD construction with width 2. A problem instance and a DD node—represented by its state and layer—are provided as input to a node-selection heuristic. Heuristics may be rule-based or learning-based; the latter include feature-engineered models and neural networks. The heuristic outputs a score for the node, which guides the construction of the width-restricted DD. The heuristic components depicted in the figure are highlighted with a dashed border.

to them, the enumeration of the Pareto frontier would be substantially faster, as it dramatically reduces the number of nodes that must be explored.

Contributions. Building on these conceptual and empirical insights, we tackle the challenge of rapidly generating a high-quality approximation of the Pareto frontier by constructing restricted DDs that retain most Pareto nodes. We develop two families of node-selection heuristics (NOSHs) to guide the restriction process: rule-based and learning-based. Figure 2 illustrates our methods.

Rule-based heuristics do not require prior knowledge about the distribution of problem instances and operate on each instance independently. For example, in the MOKP, the DD state is equal to the knapsack weight. A simple rule is to sort the nodes in each layer by decreasing weight and select only the top-ranked nodes up to the width limit.

In contrast, learning-based heuristics assume access to a sufficiently large collection of training instances, along with their Pareto frontiers, from which a binary classifier can be learned. Nodes that are predicted to be Pareto are then prioritized over the ones that are not. Once trained, the classifier is invoked on each node of the DDs of previously unseen instances that are similar in structure to those seen in training.

We demonstrate that NOSHs effectively identify Pareto nodes, leading to much faster solution enumeration compared to exact DDs and recovering a large fraction of the true Pareto frontier on three representative multiobjective problems: MOKP, MOSPP, and MOTSP.

2 Preliminaries

2.1 Multiobjective Integer Linear Programming

We define an MOILP with K objectives as $\mathcal{P} \equiv \min_x \{Cx : x \in \mathcal{X} \subseteq \mathbb{Z}^N\}$, where x is the decision vector, \mathcal{X} is the feasible set, $C \in \mathbb{R}^{K \times N}$ is the objective coefficient matrix. Let $\mathcal{Z} = \{Cx : x \in \mathcal{X}\}$ denote the set of feasible objective vectors. For two vectors $z^1, z^2 \in \mathbb{R}^K$, we say z^1 *dominates* z^2 (denoted $z^1 \prec z^2$) if $z_k^1 \leq z_k^2$ for all $k \in \{1, \dots, K\}$ and $z^1 \neq z^2$. A vector $z \in \mathcal{Z}$ is *nondominated* if there exists no $z' \in \mathcal{Z}$ such that $z' \prec z$. Solving the MOILP amounts to finding the *Pareto frontier* $\mathcal{Z}^* = \{z \in \mathcal{Z} \mid \nexists z' \in \mathcal{Z} \text{ such that } z' \prec z\}$, which is the set of all nondominated vectors. The set of feasible decision vectors that map to the Pareto frontier is defined as the *efficient set* $\mathcal{X}^* = \{x \in \mathcal{X} \mid Cx \in \mathcal{Z}^*\}$.

2.2 Decision Diagrams

A DD for problem \mathcal{P} is a layered directed acyclic graph $\mathcal{B} = (\mathcal{N}, \mathcal{A})$ with node set \mathcal{N} and arc set \mathcal{A} . The node set is partitioned into $N + 1$ layers, $\mathcal{N} = \mathcal{L}_1 \cup \dots \cup \mathcal{L}_{N+1}$. Layers \mathcal{L}_1 and \mathcal{L}_{N+1} contain only the single *root node* \mathbf{r} and *terminal node* \mathbf{t} , respectively. The *width* of the DD is the maximum size of any layer, denoted $\omega(\mathcal{B}) = \max_j |\mathcal{L}_j|$. For example, the exact DD in Figure 1 has 4 layers and a width of 4.

Arcs are directed from layer j to $j + 1$ for $j \in \{1, \dots, N\}$. For each arc $a \in \mathcal{A}$ originating from a node in \mathcal{L}_j , we define two attributes. An *assignment value* $d(a) \in \mathbb{Z}$, representing the value assigned to decision variable x_j . An *objective weight* $v(a) \in \mathbb{R}^K$, representing the contribution of this assignment to the objective function. A path $p = (a_1, \dots, a_N)$ from \mathbf{r} to \mathbf{t} defines a complete solution $x(p) = (d(a_1), \dots, d(a_N)) \in \mathbb{Z}^N$ with an associated objective vector $v(p) = \sum_{i=1}^N v(a_i)$. For instance, the path $(\mathbf{r} - 3, 3 - 4, 4 - \mathbf{t})$ in the exact DD of Figure 1 corresponds to the decision vector $(x_1, x_2, x_3) = (1, 1, 0)$ and achieves an objective of $(11, 5)$.

Let $\mathcal{X}_{\mathcal{B}} = \{x(p) : p \text{ is an } \mathbf{r}\text{-}\mathbf{t} \text{ path in } \mathcal{B}\}$ be the set of solutions encoded by the DD. The DD is *exact* for problem \mathcal{P} if $\mathcal{X}_{\mathcal{B}} = \mathcal{X}$ and the arc weights satisfy $v(p) = Cx(p)$ for all paths. Under these conditions, the image of $\mathcal{X}_{\mathcal{B}}$ in objective space is $\mathcal{Z}_{\mathcal{B}} = \{v(p) : p \text{ is an } \mathbf{r}\text{-}\mathbf{t} \text{ path}\}$. The nondominated vectors in $\mathcal{Z}_{\mathcal{B}}$ are denoted by $\mathcal{Z}_{\mathcal{B}}^*$ and is equal to the Pareto frontier \mathcal{Z}^* of \mathcal{P} .

A decision diagram \mathcal{B}' is said to be *restricted* for problem \mathcal{P} if it encodes a subset of the feasible solutions, i.e., $\mathcal{X}_{\mathcal{B}'} \subseteq \mathcal{X}$. In practice, restricted DDs are often maintained by imposing a *maximum width* W on the graph. During construction, if the number of nodes in a layer \mathcal{L}_j exceeds W , a heuristic filtering procedure is triggered. This procedure retains a subset of W nodes and removes the rest, ensuring that $\omega(\mathcal{B}') \leq W$. Consequently, the image of the feasible set $\mathcal{Z}_{\mathcal{B}'}$ is a subset of the objective space \mathcal{Z} . The nondominated vectors in $\mathcal{Z}_{\mathcal{B}'}$ are represented by $\mathcal{Z}_{\mathcal{B}'}^*$, which is an approximate Pareto frontier of \mathcal{P} .

To construct a DD we leverage the dynamic programming formulation of the problem. As a result, each node $u \in \mathcal{N}$ is associated with a *state* $s(u)$ from a state space \mathcal{S} given by the formulation. The state plays a key role in the design of NOSH for constructing restricted DDs. We refer the reader to [4, 3] for additional details on dynamic programming formulation and Pareto frontier enumeration using the multicriteria shortest path algorithm. The notation used to define MOILP and DDs is summarized in Section A.

3 Methodology

The central challenge in solving MOILPs via DDs is the exponential growth of the state space \mathcal{S} with problem size. To address this, we propose NOSHs, a framework for constructing restricted DDs that prioritize the retention of Pareto nodes, which typically form a small fraction of the total nodes as highlighted in Table 1. Given a maximum width W , our goal is to construct a restricted DD \mathcal{B}' such that $\omega(\mathcal{B}') \leq W$ while maximizing the approximation quality of the Pareto frontier.

We formalize this using a generic node scoring framework described in Section 3.1, and subsequently detail how this framework specializes into rule-based heuristics, classical machine learning with feature engineering, and end-to-end deep learning.

3.1 Node Selection Heuristics

When the width of a layer \mathcal{L}_j exceeds the maximum width W , a filtering procedure must select a size- W subset of nodes to retain. We unify this selection process under a single scoring entity, denoted as the *scorer* S_{Θ} . The scorer is a function $S_{\Theta} : \mathcal{S} \setminus \{\mathbf{s}(\mathbf{r}), \mathbf{s}(\mathbf{t})\} \times \{2, \dots, N\} \rightarrow [0, 1]$ parameterized by Θ . This function maps the state and layer index of a node $u \in \mathcal{N} \setminus \{\mathbf{r}, \mathbf{t}\}$'s, $(s(u), l(u))$ to a score representing the likelihood of u being a Pareto node.

Our objective is to learn (or design) parameters Θ that maximize the expected recovery of the exact Pareto frontier \mathcal{Z}^* . Let $\mathcal{Z}_{\mathcal{B}'(S_{\Theta})}^*$ denote the approximate Pareto frontier obtained from a restricted DD constructed using scorer S_{Θ} . The optimization objective is:

$$\max_{\Theta} \mathbb{E}_{\mathcal{P}} \left[\frac{|\mathcal{Z}_{\mathcal{B}'(S_{\Theta})}^* \cap \mathcal{Z}^*|}{|\mathcal{Z}^*|} \right], \quad (1)$$

where the expectation is taken over a distribution of training instances. An ideal scoring function achieves an objective of 1; scoring functions that eliminate too many Pareto nodes achieve a low score, as many of the returned solutions would be dominated. Based on the structure of S_{Θ} and the nature of Θ , we categorize NOSHs into three distinct approaches.

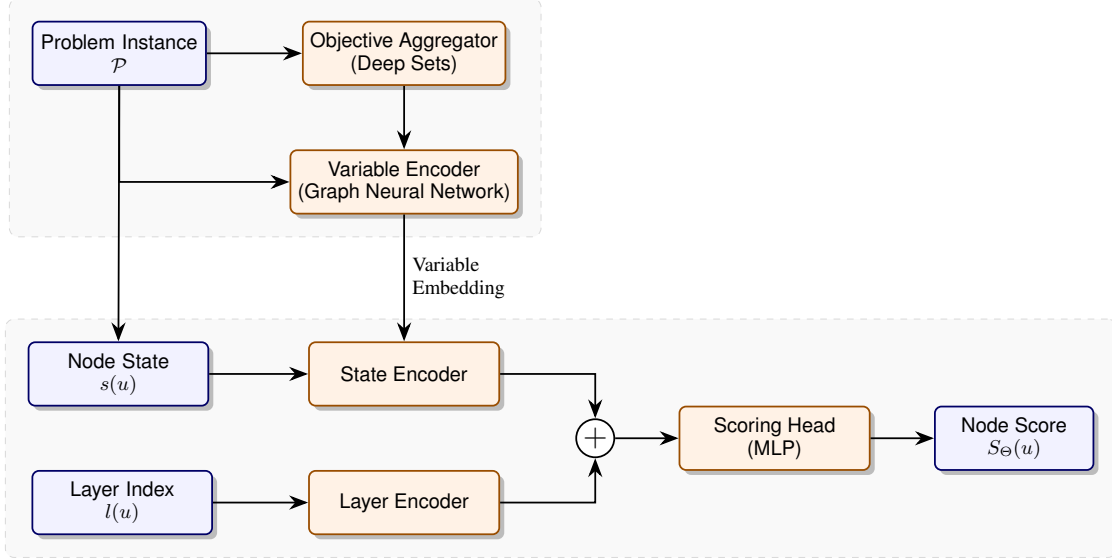


Figure 3: The generic end-to-end node selection heuristic architecture.

Rule-based scoring. In this setting, S_Θ is a fixed, deterministic function where $\Theta = \emptyset$ (i.e., there are no learnable parameters). These heuristics rely on domain knowledge and intrinsic properties of the state, as illustrated below for example.

- *Scalar States:* If $s(u) \in \mathbb{R}$, natural candidates for the scorer are the state value itself ($S(u) = s(u)$, denoted `Sca1+`) or its negation. For example, the state in MOKP is the total weight of the items that are selected in the state. Since the objectives are in the maximization direction, states that include many items can be thought to be conducive to high-quality solutions, leading to a natural scoring rule.
- *Set-based States:* If $s(u)$ is a set, the scorer may utilize the cardinality of the set ($S(u) = |s(u)|$, denoted `Card+`) or its negation. For example, the state in MOSPP is the set of items that can be added to already-selected items without violating any of the packing constraints. The larger this set, the more items one can potentially add down the line, the larger the objective values.

While computationally inexpensive, these rules are rigid and their performance sensitive to instance structure.

Learning-based scoring with feature engineering. Here, the scorer is a composite function $S_\Theta(u) = f_\Theta(\psi(s(u), l(u)))$. A fixed extraction function ψ maps the raw state and layer to a hand-crafted feature vector in \mathbb{R}^d . These features capture our understanding of the problem. A parameterized binary classification model $f_\Theta : \mathbb{R}^d \rightarrow [0, 1]$ (e.g., Logistic Regressor, Random Forest) maps these features to a probability score. In this context, Θ represents the parameters of the classifier f . This approach adapts to data but is limited by the expressiveness of the feature map ψ .

End-to-end Learning-based scoring. To overcome the limitations of manual feature engineering and capture the complex dependencies between objectives, constraints, and decision variables, we propose a generic end-to-end deep learning architecture. The scorer S_Θ maps the raw state and layer definition $(s(u), l(u))$ directly to a score. As illustrated in Figure 3, this architecture operates in two distinct phases: a computationally intensive *Instance Embedding Phase* performed once per problem instance, and a lightweight *Scoring Phase* performed for each node in the decision diagram.

The instance embedding phase begins with *Objective Aggregator*. Since the order of objectives is arbitrary, it combines information across objectives into a permutation-invariant representation using Deep Sets [38]. The key result in [38] establishes that any permutation-invariant function f mapping a set O to a representation can be approximated in the form $f(O) = \rho(\sum_{x \in O} \gamma(x))$, where γ and ρ are flexible functions (e.g., neural networks).

The *Variable Encoder*, initialized with the aggregated embeddings from the previous step, captures the intricate dependencies among various components of the problem instance. We exploit the fact that the MOILP can be represented as a graph and use a Graph Neural Network (GNN) to process it. This results in *variable embeddings* that encapsulate the

instance’s structural information. Crucially, the variable embeddings are computed only once per instance, avoiding redundant computations per DD node.

Later, these pre-computed variable embeddings are combined with dynamic state information to obtain a *State Embedding*. Finally, the state embedding is combined with a *Layer Embedding* (derived from the layer index) to obtain a comprehensive *DD Node Embedding*. This embedding is used by the *Scoring Head* to output a scalar score for a DD node.

3.2 Training Formulation

For the learning-based approaches, we employ supervised learning. We generate a node-wise training dataset \mathcal{D} derived from m problem instances. For each instance i , we use the ground-truth efficient set \mathcal{X}_i^* to label the nodes in the DD \mathcal{N}_i . The dataset is defined as the union of these labeled nodes:

$$\mathcal{D} = \{(\mathcal{P}_i, s(u), l(u), y_u) \mid i \in \{1, \dots, m\}, u \in \mathcal{N}_i\}, \quad (2)$$

where $y_u \in \{0, 1\}$ is the binary label indicating whether u is a Pareto node.

We seek parameters Θ^* that minimize the empirical risk over \mathcal{D} using the weighted binary cross-entropy loss:

$$\Theta^* \in \arg \min_{\Theta} \frac{1}{|\mathcal{D}|} \sum_{(\cdot, y_u) \in \mathcal{D}} \mathcal{L}_{\text{WBCE}}(S_{\Theta}(s(u), l(u)), y_u), \quad (3)$$

where $\mathcal{L}_{\text{WBCE}}(p, y) = -\alpha \cdot y \log p - (1 - y) \log(1 - p)$ and $\alpha \in \mathbb{R}_+$. By minimizing this loss, S_{Θ} learns to assign higher probabilities to Pareto nodes.

3.3 Case Study: Multiobjective Traveling Salesperson Problem

In the dynamic programming formulation for the MOTSP [8], a node u at layer j represents a partial tour of length $j - 1$. The state $s(u)$ is defined as the tuple $s(u) = (V_u, i)$, where $V_u \subseteq \mathcal{V}$ is the set of vertices visited on the path from the root to u , and $i \in V_u$ is the index of the last vertex added to the path (i.e., the current city). At the root node \mathbf{r} (layer 1), the state is $(\{1\}, 1)$, assuming the tour always starts at vertex 1. For a node u with state (V_u, i) , a transition to vertex j is valid if $j \notin V_u$. The succeeding state is $(V_u \cup \{j\}, j)$. The travel costs associated with different edges are represented using a matrix c , where c_{ij}^k denotes the cost of edge (i, j) for the k -th objective.

3.3.1 Rule-based Heuristics

Our rule-based heuristics leverage the edge cost matrices c^k to estimate the quality of a state. Due to the conflicting nature of the K objectives, we first compute the *rank* of each edge for every objective. Let $R \in \mathbb{R}^{N \times N \times K}$ be a tensor where R_{ijk} is the rank of cost c_{ij}^k among all edges for objective k . We derive a scalar score for node u by aggregating these ranks. First, we aggregate across objectives to obtain a single “cost” matrix $R^{\text{agg}} \in \mathbb{R}^{N \times N}$. The entry corresponding to edge (i, j) is given by $R_{ij}^{\text{agg}} = \bigoplus_1 \{R_{ijk} : k \in \{1, \dots, K\}\}$, where \bigoplus_1 is an aggregation function (e.g., mean, maximum or minimum).

The score for a node u with state (V_u, i) is determined by the potential extensions to the set of unvisited cities $U_u = \mathcal{V} \setminus V_u$. Specifically, the score is computed as $S(u) = \bigoplus_2 \{R_{ij}^{\text{agg}} : j \in U_u\}$, where $\bigoplus_2 \in \{\text{high}, \text{low}\}$ determines whether we prioritize the best or worst immediate extension¹. We denote these heuristics using the prefix “Ord” followed by the aggregation method and the prioritization direction. For instance, OrdMeanHigh aggregates ranks using the mean (\bigoplus_1) and scores the node based on the most favorable (higher rank) extension (\bigoplus_2). Conversely, a suffix of “Low” implies prioritizing edges with lower aggregated ranks (worst extensions).

3.3.2 Learning-based Heuristic

For the learning-based approach, we instantiate the end-to-end architecture proposed in Figure 3. In the instance embedding phase, the input to the objective aggregator are the node features $h_i^{v,0} \in \mathbb{R}^{N \times d_{\text{node}}}$ edge features $h_{ij}^{e,0} \in \mathbb{R}^{N \times N \times K}$. The node features are initialized with the 2D coordinates of the cities and may optionally include hand-crafted features. The edge features are initialized using the cost matrices across the K objectives, where $h_{ijk}^{e,0} = c_{ij}^k$. The objective aggregator transforms these features $h^{v,0}$ and $h^{e,0}$ into objective-invariant embeddings $h^{v,1} \in \mathbb{R}^{N \times d_{\text{emb}}}$ and $h^{e,1} \in \mathbb{R}^{N \times N \times d_{\text{emb}}}$.

¹For two ranks $r_1, r_2 \in \mathbb{R}_+$, rank r_1 is higher than r_2 if $r_1 < r_2$.

To capture the complex structural dependencies of the TSP, we utilize an Edge-augmented Graph Transformer (EGT) [20]. The EGT extends the standard Transformer by introducing *edge channels* that evolve structurally aware edge embeddings alongside node embeddings. Let $h^{v,\ell-1} \in \mathbb{R}^{N \times d_{\text{emb}}}$ and $h^{e,\ell-1} \in \mathbb{R}^{N \times N \times d_{\text{emb}}}$ denote the node and edge embeddings input to layer ℓ . We first linearly transform these embeddings using learnable weight matrices. For a single attention head with dimension d_k , we compute the query $Q^\ell = h^{v,\ell-1}W_Q^\ell$, key $K^\ell = h^{v,\ell-1}W_K^\ell$, value $V^\ell = h^{v,\ell-1}W_V^\ell$, structural bias $E^\ell = h^{e,\ell-1}W_E^\ell$, and gate $G^\ell = h^{e,\ell-1}W_G^\ell$ matrices, where $W_Q^\ell, W_K^\ell, W_V^\ell \in \mathbb{R}^{d_{\text{emb}} \times d_k}$ are the node projection matrices and $W_E^\ell, W_G^\ell \in \mathbb{R}^{d_{\text{emb}} \times 1}$ are the edge projection matrices. Consequently, the resulting matrices have dimensions $Q^\ell, K^\ell, V^\ell \in \mathbb{R}^{N \times d_k}$ and $E^\ell, G^\ell \in \mathbb{R}^{N \times N}$. The edge-augmented attention $A^\ell \in \mathbb{R}^{N \times N}$ is computed by modulating the standard dot-product similarity with the edge-derived bias and gating terms as follows:

$$A^\ell = \text{softmax}\left(\hat{H}^\ell\right) \odot \sigma(G^\ell), \quad (4)$$

$$\hat{H}^\ell = \text{clip}\left(\frac{Q^\ell(K^\ell)^T}{\sqrt{d_k}}\right) + E^\ell, \quad (5)$$

where $\sigma(\cdot)$ is the sigmoid function and \odot denotes element-wise multiplication. Here, E^ℓ acts as a structural bias added to the node affinities, while G^ℓ gates the attention values, controlling the information flow based on edge attributes.

The node embeddings are updated by aggregating V^ℓ weighted by A^ℓ . In practice, this operation is performed by multiple heads in parallel, and their outputs are combined and projected to form the input for the next layer. We stack L such layers to obtain the final instance-specific embeddings $h^{v,L}$ which acts as the variable embedding $h_{\text{emb}}^v \in \mathbb{R}^{N \times d_{\text{emb}}}$.

The primary challenge in the node scoring phase is to efficiently map the dynamic DD state $s(u) = (V_u, i)$ to a vector representation using the pre-computed embeddings h_{emb}^v . We represent the set of visited nodes V_u by modifying the variable embeddings. We define a state mask $M \in \mathbb{R}^{N \times d_{\text{emb}}}$ with learnable parameters θ_{vis} and θ_{unvis} . The mask for vertex j is set to θ_{vis} if $j \in V_u$ and θ_{unvis} otherwise. This mask is added element-wise to the variable embeddings: $h_{\text{mask}}^v = h_{\text{emb}}^v + M$. The resulting set of embeddings is then aggregated into a single vector $h_{\text{vis}} \in \mathbb{R}^{d_{\text{emb}}}$ using a Deep Sets-based network [38], capturing the composition of the partial tour regardless of visit order. To explicitly capture the current position in the graph, we extract the embedding corresponding to the last visited vertex i : $h_{\text{last}} = h_{\text{emb}}^v[i]$.

Finally, the current layer index $l(u)$ is projected to an embedding $h_{\text{layer}} \in \mathbb{R}^{d_{\text{emb}}}$ via a *Layer Encoder*, a multi-layered perceptron (MLP). The DD node representation is the sum of these embeddings $h_{\text{node}} = h_{\text{vis}} + h_{\text{last}} + h_{\text{layer}}$. This vector is passed to the scoring head (an MLP) to predict the likelihood of node u leading to a Pareto-optimal solution.

4 Computational Setup

We test the proposed approach on MOSPP, MOKP and MOTSP. We use a computing cluster with Intel Xeon CPU E5-2683 CPUs, a memory limit of 16GB, and a time limit of 1800 seconds. The DD manipulation code responsible for generating exact, restricted, or reduced DDs is based on [3]. We create a Python binding for this C++ code using pybind11. The problem definition and instance-generation scheme are detailed in Section B.

For the learning-based NOSH, each problem class and instance size has 1000 training, 100 validation, and 100 testing instances. We compute the Pareto frontier using the exact DD and extract all Pareto nodes. As shown in Table 1, Pareto nodes constitute only a small fraction of total nodes, leading to a significant class imbalance. To address this during dataset construction, we apply undersampling to the negative class: for each Pareto (positive) node, we randomly sample one non-Pareto (negative) node, resulting in a 1:1 ratio between positive and negative samples. This not only creates a balanced dataset but also limits its size, making the training tractable.

Node Selection Heuristics and Baselines As highlighted in Section 3, NOSHs can be categorized into three distinct types. We refer to the rule-based heuristic as NOSH-Ru1e, the learning-based approach that relies on feature engineering as NOSH-ML-FE and the approach that learns the scoring function end-to-end using deep learning as NOSH-ML-E2E. The NOSH-ML-E2E is the most extensible method to other problem classes among the proposed NOSHs. By modeling the MOILP as a graph, modern deep learning architectures can be leveraged to learn rich representations for scoring DD nodes. However, this expressivity incurs the computational cost of training deep learning models with multiple hyperparameters. Consequently, we adopt a complexity-aware strategy: we prioritize the lightweight NOSH-Ru1e, employing learning-based variants only when the problem complexity necessitates it. The state definition along with the implementation details of various NOSHs is provided in Section C. The approach for selecting the width for restricted DDs is given in Section D.1.

The learning-based NOSH approach for the MOKP leverages XGBoost 2.0.1 [14], a highly efficient implementation of gradient-boosted decision trees. The primary motivation for choosing XGBoost lies in its ability to deliver strong

performance with minimal tuning when meaningful, hand-crafted node features are available. Compared to neural network-based methods, this allows for more interpretable and computationally efficient models. We perform a grid search to select the best-performing model based on validation accuracy, which is then used for evaluation on the test set. The selected models achieve classification accuracies between 85% and 88% using a threshold of $\tau = 0.5$ on the predicted scores. The corresponding mean absolute errors fall within the range of 0.18 to 0.23. In contrast, designing hand-crafted features for the MOTSP is considerably more challenging. Therefore, to develop an end-to-end node scoring model for this setting, we employ a graph transformer implemented using PyTorch [32]. Details of the hyperparameters used for the node scorers are provided in Section D.2.

Our primary baseline is the state-of-the-art exact DD method (referenced as Exact) based on coupled enumeration [3]. We also benchmarked against NSGA-II. Despite its widespread use, NSGA-II failed to produce high-quality approximations of the Pareto frontier, even with increased runtime. When the population size was scaled to match that of the Exact method, it struggled to find feasible solutions. With smaller, more typical population sizes, the resulting frontier was consistently of lower quality than those obtained by NOSH-based approaches. Consequently, we focus our analysis on the DD-based comparisons. Detailed experimental settings and the supplementary NSGA-II analysis are available in Section E.

Metrics We report the following metrics to evaluate and compare the performance of different methods.

1. **Width:** The width of the constructed DDs. Ideally, smaller restricted DDs are preferred, provided they still capture most of the Pareto frontier.
2. **Time:** The total time (in seconds) required to construct the DD and enumerate the Pareto frontier. Faster methods are desirable, especially when approximating the frontier for large or complex instances. Note that the time required to compile the DD is a small fraction of the total time, even for the learning-based NOSH. Therefore, we report only the total time for constructing the DD and enumerating the Pareto frontier.
3. **Cardinality:** The fraction of true Pareto-optimal solutions captured by a method, relative to the total number of Pareto-optimal solutions. Let $\hat{\mathcal{Z}}^*$ denote the set of solutions obtained by a given method. Then, cardinality is computed as $(|\hat{\mathcal{Z}}^* \cap \mathcal{Z}^*|/|\mathcal{Z}^*|) \times 100$. A higher cardinality indicates that a larger portion of the true Pareto frontier is recovered.
4. **Precision:** The fraction of solutions identified by the method that are truly Pareto-optimal. This is calculated as $(|\hat{\mathcal{Z}}^* \cap \mathcal{Z}^*|/|\hat{\mathcal{Z}}^*|) \times 100$. A higher precision suggests that the approximate Pareto frontier consists predominantly of true Pareto-optimal solutions.
5. **Inverted Generational Distance (IGD) [15]:** The average distance from each solution in \mathcal{Z}^* to its closest solution in $\hat{\mathcal{Z}}^*$. Lower IGD values indicate a closer and more comprehensive approximation of the true Pareto frontier. To ensure scale invariance across objectives, we normalize each objective using the minimum and maximum values observed in \mathcal{Z}^* before computing IGD.

5 Results

Evidently, some restricted DDs are better than others in that they approximate the true Pareto frontier more completely. We will show how NOSHs finds such “accurate” restricted DDs for MOSPP, MOKP and MOTSP in Section 5.1, Section 5.2 and Section 5.3, respectively. The metrics Width, Cardinality, Precision and $|\hat{\mathcal{Z}}^*|$ are rounded to the nearest integer, whereas Time is rounded up. In all tables, the Exact method is shown in gray as a reference baseline and is not included in the comparative evaluation, as it represents the ground-truth Pareto frontier.

5.1 Multiobjective Set Packing Problem

Table 2 reports the performance of Exact and NOSH-Ru1e for the MOSPP. The method NOSH-Ru1e is based on the Card+ heuristic detailed in Section 3.1. The NOSH-Ru1e has Cardinality and Precision in the range of $\sim 85\%$ to 99% and $\sim 90\%$ to 99% , respectively. NOSH-Ru1e achieves up to $11\times$ speedup over Exact, with most instances exhibiting $2\times-7\times$ improvements.

For larger instances ($N = 150$ and $K \geq 5$), the reported metrics are averaged over fewer than 100 test instances. This is because the Exact method often exceeds the memory limit as instance size increases, making it unable to compute the Pareto frontier for all cases. Consequently, we apply NOSH-Ru1e only to those instances where Exact completes within the time and memory constraints, which explains the value of “Inst.” being less than 100. Note that applying learning-based NOSH would be a challenge in this setting as it would depend on labeled training data, which limits its

Table 2: MOSPP results averaged over “Inst.” test instances. Each column corresponds to a specific instance size (N, K) , with rows giving the metrics for the Exact and NOSH-Rule methods. Refer to Section 4 for column description.

Metric	Method	$N = 100$					$N = 150$				
		$K = 3$	$K = 4$	$K = 5$	$K = 6$	$K = 7$	$K = 3$	$K = 4$	$K = 5$	$K = 6$	$K = 7$
Width	Exact	5,766	6,034	5,936	5,976	5,707	471,602	518,556	464,330	468,787	590,908
	NOSH-Rule	50	50	50	50	50	5,000	5,000	5,000	5,000	5,000
Time ↓	Exact	1	1	2	5	31	11	51	261	567	783
	NOSH-Rule	1	1	1	2	13	1	7	77	183	314
Cardinality ↑	Exact	100	100	100	100	100	100	100	100	100	100
	NOSH-Rule	85	84	89	87	87	99	99	99	99	99
Precision ↑	Exact	100	100	100	100	100	100	100	100	100	100
	NOSH-Rule	89	90	94	94	93	100	100	99	100	100
IGD ↓	Exact	0.000	0.000	0.000	0.000	0.000	0.000	0.000	0.000	0.000	0.000
	NOSH-Rule	0.012	0.016	0.013	0.017	0.019	0.000	0.000	0.001	0.001	0.001
$ \hat{\mathcal{Z}}^* $	Exact	238	1,117	4,765	9,117	25,457	787	6,099	29,061	59,951	103,489
	NOSH-Rule	226	1,051	4,591	8,550	24,534	786	6,089	28,953	59,724	103,275
Inst.		100	100	100	100	100	100	100	92	54	27

Table 3: MOKP results averaged across 100 test instances. Refer to Section 4 for column description.

N	K	Method	Width	Time ↓	Cardinality ↑	Precision ↑	IGD ↓	$ \hat{\mathcal{Z}}^* $
40	7	Exact	9,709	84	100	100	0.000	25,098
		NOSH-Rule	2,000	2	19	64	0.128	4,131
			3,000	19	61	89	0.047	12,972
	NOSH-ML-FE	2,000	16	60	74	0.042	20,482	
		3,000	36	88	96	0.012	22,267	
50	4	Exact	12,359	7	100	100	0.000	3,564
		NOSH-Rule	2,500	1	17	36	0.085	1,132
			3,500	2	52	70	0.032	2,256
	NOSH-ML-FE	2,500	3	61	70	0.020	3,062	
		3,500	4	88	92	0.006	3,367	
80	3	Exact	20,097	27	100	100	0.000	2,442
		NOSH-Rule	4,000	3	10	19	0.064	1,015
			6,000	7	62	71	0.013	1,954
	NOSH-ML-FE	4,000	6	46	53	0.012	2,039	
		6,000	12	93	95	0.002	2,363	

Table 4: MOTSP results averaged across 100 test instances. Refer to Section 4 for column description.

N	K	Method	Width	Time ↓	Cardinality ↑	Precision ↑	IGD ↓	$ \hat{\mathcal{Z}}^* $
15	3	Exact	24,024	3	100	100	0.000	868
		NOSH-Rule	4,804	2	1	2	0.085	439
			NOSH-ML-E2E	4,804	2	91	95	0.003
	4	Exact	24,024	28	100	100	0.000	9,210
		NOSH-Rule	4,804	3	1	4	0.082	3,254
			NOSH-ML-E2E	4,804	13	89	95	0.004

applicability to larger instances as we do not have access to the exact Pareto frontier. In summary, NOSH-Rule achieved a good trade-off between solution quality and enumeration time, without the need for expensive data labeling.

5.2 Multiobjective Knapsack Problem

The performance of different approaches for the MOKP is presented in Table 3. The `NOSH-Rule` method, derived from the `Scal+` heuristic (Section 3.1), is sensitive to the width of the restricted DD, with Cardinality and Precision ranging from 52%–62% and 69%–89%, respectively. In contrast, `NOSH-ML-FE` consistently outperforms `NOSH-Rule`, achieving Cardinality between 87%–92% and Precision between 92%–95%, along with lower IGD values. Moreover, `NOSH-ML-FE` attains speedups of $1.75\times$ – $2.33\times$ over Exact in most settings. Overall, these results highlight the advantage of `NOSH-ML-FE` in achieving superior trade-offs between solution quality and runtime. Additionally, the use of XGBoost with handcrafted features enhances interpretability by enabling identification of the most influential features.

5.3 Multiobjective Traveling Salesperson Problem

The results for MOTSP are presented in Table 4. The `NOSH-Rule` method, based on the `OrdMeanLow` heuristic, achieves significant speedups but performs poorly in terms of solution quality, with Cardinality and Precision close to zero and relatively high IGD values, indicating a weak approximation of the Pareto frontier. In contrast, `NOSH-ML-E2E` substantially improves solution quality, achieving Cardinality between 89%–91% and Precision around 95%, along with very low IGD values. It also attains speedups of $1.5\times$ – $2.15\times$ compared to the Exact method. These results demonstrate that `NOSH-ML-E2E` is effective in learning useful node representations from raw data and accurately identifying Pareto-optimal nodes.

6 Related Work

As surveyed in [18, 17], the literature on exact approaches to MOILPs is vast and generally partitioned into decision space methods [1] and objective space methods [10, 11]. The former searches in the space of feasible solutions whereas the latter search in the space of objective vectors. Many of these approaches are confined to biobjective and triobjective problems. Notable exceptions include the KSA algorithm [23] and the DD approach [4]. The latter has been shown to outperform KSA by a substantial margin on combinatorial problems that are amenable to a dynamic programming formulation, which is why we focus on this promising algorithmic paradigm in this work. Specifically, our approach allows efficient state-space exploration, similar to [24], by eliminating states less likely to contribute to a Pareto optimal solution. Note that the authors of [4] enhance a basic decision diagram approach in [3] by introducing a series of Pareto frontier preserving operations. Those would directly apply here, but we utilize the basic decision diagram approach for transparency and ease of implementation.

Evolutionary or genetic algorithms (GAs) have long been used for multiobjective optimization. The Pymoo paper and software package [9] summarize and implement state-of-the-art GAs such as NSGA-II. Note that the NSGA-II [16] is widely used (45,000+ citations) so outperforming it is a good sanity check of the promise of any new method. However, it is known that GAs typically struggle with integer variables and hard constraints, a limitation that is not exhibited by the DD approach. Another class of heuristics based on integer and linear programming appear in [30, 31, 2]. They extended the single-objective “Feasibility Pump” [19] heuristic to the multiobjective case. The method in [2] is evaluated only on triobjective problems with binary variables whereas `NOSH` will be applied to problems with more objective and discrete variables, a substantial generalization. With the expansive literature on heuristic approaches to MOILP, we opted to compare only with NSGA-II as it is the best known and has been a strong competitor and benchmark comparison algorithm for over two decades.

Relative to single-objective optimization, there has been much less work on ML for multiobjective discrete optimization. ML-based methods have been proposed for unconstrained continuous multiobjective problems that arise in deep learning applications such as multi-task learning [28] or molecule generation [21, 26]. Because they are not equipped to deal with hard constraints, these methods do not apply to combinatorial optimization. More relevant to this paper is the work of [37] who train a *graph neural network* (GNN) to guide the exact algorithm of [35]. This GNN-based method is evaluated on knapsack problems with 3-5 objectives only and requires a much larger amount of time than `NOSH`. For example, on instances with 4 objectives and 50 variables, `NOSH` runs in about 11 seconds on average (Table 3) whereas the method in [37] (Table 1) runs for 1,000 seconds on a faster CPU than ours. Additionally, no publicly available code was provided for this rather sophisticated GNN architecture, making a direct comparison challenging.

7 Conclusion and Future Work

We demonstrated the use of restricted DDs as a heuristic to solve multiobjective integer linear programming problems. In fact, to the best of our knowledge, we are the first to invoke restricted DDs in the context of multiobjective

optimization as they have only appeared in the single objective case. We presented two types of node selection heuristics, rule-based and learning-based, to construct the restricted DDs for the MOKP, MOSPP and MOTSP. The results demonstrate that node selection heuristics provide a high-quality approximation of the true Pareto frontier and are significantly faster than the exact DDs. Specifically, NOSH-Ru1e, NOSH-ML-FE and NOSH-ML-E2E performed exceedingly well for the MOSPP, MOKP and MOTSP, respectively.

Furthermore, instead of classifying a node in isolation, one can formulate the problem of constructing the restricted DDs as a structured output prediction task. Specifically, given an exact DD the goal is to predict a subgraph consisting only of nodes and arcs used by the Pareto optimal solutions. Predicting a subgraph is a combinatorial task which has received significant attention from the machine learning community [22] but has not been applied to optimization applications such as ours here. One limitation of our approach is its reliance on the complete Pareto frontier to generate the training dataset for the learning-based node selection heuristics. In the future, we aim to relax this requirement by utilizing partial Pareto frontiers for training data generation. This relaxation may necessitate an increase in the number of training instances to maintain performance.

A Mathematical Notation

The notation used to describe MOILP and DDs is presented in Table 5 and Table 6, respectively.

Table 5: Mathematical notation for MOILP

Symbol	Description
\mathcal{P}	A multiobjective integer linear programming problem
N	Number of decision variables
K	Number of objectives
$x \in \mathbb{Z}^N$	Integer-valued decision vector
$\mathcal{X} \subseteq \mathbb{Z}^N$	Feasible solution set
$C \in \mathbb{R}^{K \times N}$	Objective function coefficient matrix
\mathcal{Z}	Set of feasible objective vectors (Image of (\mathcal{X}) in the objective space)
\prec	Dominance relation: $z^1 \prec z^2$ implies z^1 dominates z^2
$\mathcal{Z}^* \subseteq \mathcal{Z}$	Pareto frontier (set of nondominated objective vectors)

Table 6: Mathematical notation for DDs

Symbol	Description
$\mathcal{B} = (\mathcal{N}, \mathcal{A})$	A decision diagram for problem \mathcal{P}
\mathcal{N}	Set of nodes in a DD
\mathcal{A}	Set of arcs (directed edges) in a DD
\mathcal{L}_j	Set of nodes in layer j , for $j \in \{1, \dots, N + 1\}$
\mathbf{r}, \mathbf{t}	Root node (layer 1) and terminal node (layer $N + 1$)
$\omega(\mathcal{B})$	Width of the DD: $\max_j \mathcal{L}_j $
$a \in \mathcal{A}$	An arc in the DD
$d(a)$	Assignment value of arc a (value for variable x_j)
$v(a)$	Objective weight of arc a (vector in \mathbb{R}^K)
p	A path from \mathbf{r} to \mathbf{t}
$x(p)$	Solution vector encoded by path p
$v(p)$	Objective vector accumulated along path p
$\mathcal{X}_{\mathcal{B}}$	Set of feasible integer solutions encoded by \mathcal{B}
$\mathcal{Z}_{\mathcal{B}}$	Set of objective vectors encoded by \mathcal{B}
$\mathcal{Z}_{\mathcal{B}}^*$	Set of nondominated vectors in $\mathcal{Z}_{\mathcal{B}}$ (Pareto frontier)
<i>Restricted DDs and Construction</i>	
\mathcal{B}'	Restricted DD where $\mathcal{X}_{\mathcal{B}'} \subseteq \mathcal{X}$
W	Maximum width parameter for restricted DDs
$\mathcal{Z}_{\mathcal{B}'}^*$	Approximate Pareto frontier derived from \mathcal{B}'
\mathcal{S}	State space defined by the DP formulation of \mathcal{P}
$s(u) \in \mathcal{S}$	State associated with node u

B Problem Definition and Instance Generation

In this section, we provide the formulation of the MOILP problems considered in this work and corresponding instance generation scheme.

B.1 Multiobjective Travelling Salesperson Problem

B.1.1 Problem Definition

The MOTSP extends the classical traveling salesperson problem by incorporating multiple, potentially conflicting cost metrics associated with traversing arcs. We consider a complete directed graph $\mathcal{G} = (\mathcal{V}, \mathcal{E})$ where $\mathcal{V} = \{1, \dots, N\}$ is the set of vertices (cities) and $\mathcal{E} = \{(i, j) : i, j \in \mathcal{V}, i \neq j\}$ is the set of edges. There are K cost matrices, where c_{ij}^k denotes the cost of edge (i, j) for the k -th objective. The problem consists of finding a Hamiltonian cycle (a permutation of the vertices) that simultaneously minimizes the objective vectors. In the context of the MOILP formulation, the decision variables $x = (x_1, \dots, x_N) \in \mathcal{V}^N$ represent the permutation of vertices visited, such that x_j is the index of the vertex visited at step j .

B.1.2 Instance Generation

The instances are generated as in [29]. For each K , we generated integer coordinates for N cities on a 1000×1000 square (uniformly at random) and used Euclidean distances to create the distance matrix.

B.2 Multiobjective Knapsack Problem

B.2.1 Problem Definition

The MOKP involves selecting a subset of items to maximize multiple profit objectives subject to a single weight capacity constraint. Given N items, let $w \in \mathbb{Z}_+^N$ be the vector of item weights and $B \in \mathbb{Z}_+$ be the knapsack capacity. The profit of item j for the k -th objective is given by the entry C_{kj} . The problem is formulated as:

$$\max_{x \in \{0,1\}^N} \left\{ Cx \mid \sum_{j=1}^N w_j x_j \leq B \right\}.$$

Here, the decision variable $x_j = 1$ implies item j is selected, and $x_j = 0$ otherwise.

B.2.2 Instance Generation

We follow the instance generation scheme used in [23], where each profit C_{kj} and weight w_j were drawn uniformly at random from the integer interval $[1, \dots, 1000]$. The capacity of the knapsack was set to $B := \lceil 0.5 \sum_{j=1}^N w_j \rceil$.

B.3 Multiobjective Set Packing Problem

B.3.1 Problem Definition

The MOSPP seeks to select a subset of variables to maximize objectives subject to pairwise conflict constraints (or packing constraints). Let $A \in \{0, 1\}^{M \times N}$ be a binary constraint matrix with M constraints, and $\mathbf{1}$ be a vector of ones of size M . The problem is defined as:

$$\max_{x \in \{0,1\}^N} \{Cx : Ax \leq \mathbf{1}\}.$$

The constraint $Ax \leq \mathbf{1}$ implies that for any row m of A , at most one variable j with $A_{mj} = 1$ can be set to 1. This is equivalent to finding a maximum weight independent set on the intersection graph defined by A .

B.3.2 Instance Generation

The instance generation for the MOSPP is based on the previous work by [34]. Specifically, we fix the number of constraints $M = N/5$. Then for each constraint, we select the number of variables that participate in it from a random uniform distribution over $[2, 20]$, resulting in an average of 10 variables per constraint.

We identified a minor issue in this instance generation process. Specifically, certain variables were not involved in any constraints. To address this, we randomly assign such variables to any one of the existing constraints, ensuring all variables participate meaningfully in the problem formulation.

C Implementation Details of Node Selection Heuristics

In this section, we describe the implementation of the node selection heuristics for the MOKP and MOSPP. The corresponding details for the MOTSP are presented in Section 3.3.

C.1 Multiobjective knapsack problem

C.1.1 State Definition

The state $s(u)$ at layer j (where the decision for item $j - 1$ has just been made) tracks the resource consumption. It is defined as a scalar:

$$s(u) = q, \quad (6)$$

where $q \in \mathbb{Z}_{\geq 0}$ represents the accumulated weight of items selected in the path from the root to node u . Formally, if u is reached by a path p with assignments x_1, \dots, x_{j-1} , then $s(u) = \sum_{t=1}^{j-1} w_t x_t$. A transition $x_j = 1$ is feasible only if $s(u) + w_j \leq B$. If $x_j = 1$, the next state is $s(u) + w_j$; if $x_j = 0$, the next state is $s(u)$.

C.1.2 Rule-based Heuristic

As the state in MOKP is scalar-valued, the NOSH-Rule method uses Scal+ to select the nodes along with minWeight variable ordering [33]. In minWeight variable ordering, we sort the items based on the ascending order of their weight before constructing the DD.

C.1.3 Learning-based Heuristic

The features used by the NOSH-ML method are presented in Table 7. Note that these features rely on the fact that the problem has only one constraint. Extending this approach to problems with multiple constraints can be non-trivial.

Table 7: Features associated with a DD node for the MOKP.

Feature scope	Feature	Count
Instance features	The number of objectives	1
	The number of items (or variables)	1
	The capacity of the knapsack	1
	The mean, min., max., and std. of the weights	4
	The mean, min., max., and std. of the values	12
Layer-variable features	The weight associated with variable	1
	Average value across objectives	1
	Maximum value across objectives	1
	Minimum value across objectives	1
	Standard deviation across objectives	1
	Ratio of average value across objectives to weight	1
	Ratio of maximum value across objectives to weight	1
Layer-index features	Normalized layer index	1
	Normalized state (weight of the knapsack at the current node)	1
State features	Normalized state (weight of the knapsack at the current node)	1
	Ratio of state by capacity	1
Total		44

C.2 Multiobjective set packing problem

C.2.1 State Definition

The state $s(u)$ at layer j must capture the availability of the remaining variables x_j, \dots, x_N given the decisions made so far. The state is defined as the set of *eligible* variables:

$$s(u) = \mathcal{V}_{eligible} \subseteq \{j, \dots, N\}, \quad (7)$$

where $k \in \mathcal{V}_{eligible}$ implies that selecting variable k (setting $x_k = 1$) does not violate any constraints given the variables already selected in the path to u . At the root node, $s(\mathbf{r}) = \{1, \dots, N\}$. Given a node u at layer j with state $s(u)$:

- If $x_j = 0$, the constraint set remains unchanged for the remaining variables. The next state is $s(u) \setminus \{j\}$.
- If $x_j = 1$ (valid only if $j \in s(u)$), we must remove j and all future variables $k > j$ that conflict with j (i.e., variables k such that $\exists m, A_{mj} = 1 \wedge A_{mk} = 1$). The next state is $\{k \in s(u) \setminus \{j\} \mid \text{variable } k \text{ does not conflict with } j\}$.

C.2.2 Rule-based Heuristic

The NOSH-Rule method uses the Card+ heuristic to select states as they are represented as a set. Ties among nodes with the same cardinality are broken by randomly selecting a subset of them to fit the width limit. To build the DD, we use the minState [6] variable ordering, where we select the variable appearing in the minimum number of states in the current layer to construct the next layer.

D Additional Computational Details

D.1 Width Selection for Restricted DDs

One of the key considerations in constructing restricted DDs is determining its width. If the width is too small, the DD may be overly restrictive, making it difficult to recover the true Pareto frontier. Conversely, if the width is too large, the performance of the restricted DD may closely resemble that of the exact DD, offering little computational advantage.

In the DD literature, the width is typically chosen based on empirical validation, tuned to the downstream task performance using the restricted DD. In this work, we begin by setting the initial width to approximately 20% of the average width of the exact DDs for a given problem class and instance size. If the method achieves both cardinality and precision above 80%, we retain the current width. Otherwise, we incrementally increase the width budget by 10%. Conversely, if the method performs exceptionally well with the initial width, we systematically reduce it to identify a minimal effective width.

As demonstrated in Section 5, effective width budgets for the MOSPP, MOKP, and MOTSP are found to be 1%, 30%, and 20% of the average exact DD width, respectively.

D.2 Hyperparameter Configuration

Section D.2.1 provides the architectural and training details for the learning-based heuristic for the MOTSP. Section D.2.2 outlines the configuration of the learning-based heuristic for the MOKP, which is based on XGBoost. Finally, Section D.2.3 describes the parameters of the NSGA-II-based evolutionary baseline.

D.2.1 MOTSP scorer configuration

We enrich the raw vertex features of the MOTSP by computing additional features based on the distances per objective. Specifically, for each vertex, we compute the mean, minimum, maximum, standard deviation, and interquartile range (75th percentile minus 25th percentile) of the distances to other nodes for each objective. These five statistical features are concatenated with the original 2D coordinates of the vertex, resulting in a 7-dimensional feature vector for each vertex. This enhanced representation provides the model with richer contextual information about each node’s relative position and importance in the instance.

The Objective Aggregator processes this input using a Deep Sets architecture, which is permutation invariant over objectives. It transforms the enriched node features $h_0^v \in \mathbb{R}^{N \times K \times 7}$ and edge features $h_0^e \in \mathbb{R}^{N \times N \times K}$ into fixed-size embeddings $h_{agg}^v \in \mathbb{R}^{N \times 32}$ and $h_{agg}^e \in \mathbb{R}^{N \times N \times 32}$, respectively, with an embedding dimension of 32. These embeddings are then passed into the downstream Graph Transformer network.

Table 8: Hyperparameter configuration for the XGBoost-based scorers used in MOKP

Parameter	Size		
	(7, 40)	(4, 50)	(3, 80)
max_depth	9	7	5
min_child_weight	10000	10000	1000
eta	0.3		
objective	binary:logistic		
num_round	250		
early_stopping_rounds	20		
eval_metric	logloss		

Table 9: NSGA-II Configuration

Config	MOKP & MOSPP	MOTSP
Crossover	TwoPointCrossover	OrderCrossover
Mutation	BitflipMutation	InversionMutation
Sampling	BinaryRandomSampling	PermutationRandomSampling

Concretely, we define feature encoders and aggregators using functions:

$$\gamma_v : \mathbb{R}^7 \rightarrow \mathbb{R}^{32}, \quad \rho_v : \mathbb{R}^{64} \rightarrow \mathbb{R}^{32}, \quad \gamma_e : \mathbb{R} \rightarrow \mathbb{R}^{32}, \quad \rho_e : \mathbb{R}^{32} \rightarrow \mathbb{R}^{32}$$

Here, γ_v and γ_e are per-objective encoders applied independently to each node and edge for a given objective, while ρ_v and ρ_e are permutation-invariant aggregators that combine the representations across objectives. The output of this aggregation serves as a unified embedding that captures information across all objectives. These encoders and aggregators are implemented as a single linear layer with ReLU activation in the output.

The EGT is configured with 4 layers and 8 heads per layer and no dropout. The architecture uses ReLU as activation and omits biases in both multi-head attention and linear layers. A hidden-to-input dimension ratio of 2 is used in the MLP blocks. The model is trained for 100 epochs using the Adam optimizer. The learning rate is linearly warmed up from 5×10^{-5} to 5×10^{-4} , after which it follows a cosine decay schedule down to a minimum of 5×10^{-5} .

D.2.2 MOKP scorer configuration

Table 8 describes the configuration details for the XGBoost-based node scorer for MOKP, including the number of trees, learning rate, and maximum depth.

D.2.3 NSGA II Configuration

The crossover, mutation, and sampling strategies for the NSGA-II algorithm applied to different problems is provided in Table 9. For each problem type and size, we set the time budget for MOSPP, MOKP, and MOTSP to match the average runtime of NOSH-Rule, NOSH-ML-FE, and NOSH-ML-E2E, respectively. Initially, we set the population size to the average number of nondominated solutions observed for each problem size. However, this led to out-of-memory errors for some sizes, prompting us to reduce the population size accordingly.

E Additional results

Table 11, Table 12, and Table 10 present the complete NSGA-II results for MOSPP, MOKP, and MOTSP, respectively. In addition, Table 10 includes the performance of various rule-based NOSH variants explored in our experiments.

Table 10: MOTSP results averaged across test instances. Methods prefixed with Ord correspond to different rule-based NOSHS. NSGA-II- p denotes NSGA-II with population size p . Refer to Section 4 for column description.

N	K	Method	Width	Time ↓	Cardinality ↑	Precision ↑	IGD ↓	$ \hat{Z}^* $
15	3	Exact	24,024	3	100	100	0.000	868
		NSGA-II-100	–	3	4	31	3.558	100
		NSGA-II-500	–	3	7	20	3.531	278
		OrdMeanHigh	4,804	2	0	1	0.116	376
		OrdMeanLow	4,804	2	1	2	0.085	439
		OrdMaxHigh	4,804	2	0	1	0.116	366
		OrdMaxLow	4,804	2	1	3	0.090	425
		OrdMinHigh	4,804	2	0	1	0.105	369
		OrdMinLow	4,804	1	1	2	0.087	440
	NOSH-ML-E2E	4,804	2	91	95	0.003	832	
	4	Exact	24,024	28	100	100	0.000	9,210
		NSGA-II-100	–	25	0	11	4.056	100
		NSGA-II-500	–	25	2	28	4.008	500
		OrdMeanHigh	4,804	2	0	2	0.096	2,737
		OrdMeanLow	4,804	2	1	4	0.082	3,254
OrdMaxHigh		4,804	2	1	2	0.094	2,721	
OrdMaxLow		4,804	2	1	3	0.081	3,281	
OrdMinHigh		4,804	2	0	1	0.095	2,790	
OrdMinLow		4,804	2	1	2	0.084	3,229	
NOSH-ML-E2E	4,804	7	89	95	0.004	8,546		

 Table 11: MOSPP results averaged over test instances. Each column corresponds to a specific instance size (N, K) . NSGA-II- p denotes NSGA-II with population size p . Refer to Section 4 for column description.

Metric	Method	$N = 100$					$N = 150$				
		$K = 3$	$K = 4$	$K = 5$	$K = 6$	$K = 7$	$K = 3$	$K = 4$	$K = 5$	$K = 6$	$K = 7$
Width	Exact	5,766	6,034	5,936	5,976	5,707	471,602	518,556	464,330	468,787	590,908
	NSGA-II-100	–	–	–	–	–	–	–	–	–	–
	NSGA-II-500	–	–	–	–	–	–	–	–	–	–
	NOSH-Rule	50	50	50	50	50	5,000	5,000	5,000	5,000	5,000
Time ↓	Exact	1	1	2	5	31	11	51	261	567	783
	NSGA-II-100	1	1	1	2	13	1	7	77	182	313
	NSGA-II-500	1	1	1	2	13	1	7	77	182	313
	NOSH-Rule	1	1	1	2	13	1	7	77	183	312
Cardinality ↑	Exact	100	100	100	100	100	100	100	100	100	100
	NSGA-II-100	2	1	1	1	1	0	0	0	0	0
	NSGA-II-500	0	0	0	0	4	0	0	1	1	0
	NOSH-Rule	85	84	89	87	87	99	99	99	99	99
Precision ↑	Exact	100	100	100	100	100	100	100	100	100	100
	NSGA-II-100	12	15	14	30	50	0	8	24	31	38
	NSGA-II-500	0	0	0	1	56	0	1	28	36	44
	NOSH-Rule	89	90	94	94	93	100	100	99	100	100
IGD ↓	Exact	0.000	0.000	0.000	0.000	0.000	0.000	0.000	0.000	0.000	0.000
	NSGA-II-100	0.234	0.252	0.281	0.260	0.289	0.437	0.205	0.232	0.293	0.309
	NSGA-II-500	1.413	1.234	1.111	0.487	0.198	2.350	0.282	0.142	0.189	0.222
	NOSH-Rule	0.012	0.016	0.013	0.017	0.019	0.000	0.000	0.001	0.001	0.001
$ \hat{Z}^* $	Exact	238	1,117	4,765	9,117	25,457	787	6,099	29,061	59,951	103,489
	NSGA-II-100	26.7	45.8	63.8	96.6	100.0	19.6	97.7	100.0	100.0	100.0
	NSGA-II-500	6.016	9.684	15.862	45.206	445.142	0.078	74.084	499.028	499.981	499.956
	NOSH-Rule	226	1,051	4,591	8,550	24,534	786	6,089	28,953	59,724	103,275
Inst.		100	100	100	100	100	100	100	92	54	27

Table 12: MOKP results averaged across test instances. NSGA-II- p denotes NSGA-II with population size p . Refer to Section 4 for column description.

N	K	Method	Width	Time ↓	Cardinality ↑	Precision ↑	IGD ↓	$ \hat{Z}^* $
40	7	Exact	9,709	84	100	100	0.000	25,098
		NSGA-II-100	–	60	0	0	0.282	100
		NSGA-II-500	–	60	0	0	0.199	500
		NOSH-Rule	2,000	2	19	64	0.128	4,131
			3,000		61	89	0.047	12,972
		NOSH-ML-FE	2,000	16	60	74	0.042	20,482
3,000	36		88	96	0.012	22,267		
50	4	Exact	12,359	7	100	100	0.000	3,564
		NSGA-II-100	–	12	0	0	0.137	100
		NSGA-II-500	–	12	0	0	0.059	497
		NOSH-Rule	2,500	1	17	36	0.085	1,132
			3,500	2	52	70	0.032	2,256
		NOSH-ML-FE	2,500	3	61	70	0.020	3,062
3,500	4		88	92	0.006	3,367		
80	3	Exact	20,097	27	100	100	0.000	2,442
		NSGA-II-100	–	58	0	0	0.068	100
		NSGA-II-500	–	58	0	0	0.023	499
		NOSH-Rule	4,000	3	10	19	0.064	1,015
			6,000	7	62	71	0.013	1,954
		NOSH-ML-FE	4,000	6	46	53	0.012	2,039
6,000	12		93	95	0.002	2,363		

References

- [1] Nathan Adelgren and Akshay Gupte. Branch-and-bound for biobjective mixed-integer linear programming. *INFORMS Journal on Computing*, 34(2):909–933, 2022.
- [2] Duleabom An, Sophie N Parragh, Markus Sinnl, and Fabien Tricoire. A matheuristic for tri-objective binary integer linear programming. *Computers & Operations Research*, 161:106397, 2024.
- [3] David Bergman, Merve Bodur, Carlos Cardonha, and Andre A Cire. Network models for multiobjective discrete optimization. *INFORMS Journal on Computing*, 2021.
- [4] David Bergman and Andre A Cire. Multiobjective optimization by decision diagrams. In *International Conference on Principles and Practice of Constraint Programming*, pages 86–95. Springer, 2016.
- [5] David Bergman, Andre A Cire, Willem-Jan van Hoes, and John N Hooker. Optimization bounds from binary decision diagrams. *INFORMS Journal on Computing*, 26(2):253–268, 2014.
- [6] David Bergman, Andre A Cire, Willem-Jan Van Hoes, and John Hooker. *Decision diagrams for optimization*, volume 1. Springer, 2016.
- [7] David Bergman, Willem-Jan Van Hoes, and John N Hooker. Manipulating mdd relaxations for combinatorial optimization. In *International Conference on AI and OR Techniques in Constraint Programming for Combinatorial Optimization Problems*, pages 20–35. Springer, 2011.
- [8] Dimitri Bertsekas. *Dynamic programming and optimal control: Volume I*, volume 4. Athena scientific, 2012.
- [9] Julian Blank and Kalyanmoy Deb. Pymoo: Multi-objective optimization in Python. *IEEE Access*, 8:89497–89509, 2020.
- [10] Natashia Boland, Hadi Charkhgard, and Martin Savelsbergh. The triangle splitting method for biobjective mixed integer programming. In *Integer Programming and Combinatorial Optimization: 17th International Conference, IPCO 2014, Bonn, Germany, June 23-25, 2014. Proceedings 17*, pages 162–173. Springer, 2014.
- [11] Natashia Boland, Hadi Charkhgard, and Martin Savelsbergh. A criterion space search algorithm for biobjective integer programming: The balanced box method. *INFORMS Journal on Computing*, 27(4):735–754, 2015.
- [12] Randal E Bryant. Graph-based algorithms for boolean function manipulation. *Computers, IEEE Transactions on*, 100(8):677–691, 1986.

- [13] Quentin Cappart, Emmanuel Goutier, David Bergman, and Louis-Martin Rousseau. Improving optimization bounds using machine learning: Decision diagrams meet deep reinforcement learning. In *Proceedings of the AAAI Conference on Artificial Intelligence*, volume 33, pages 1443–1451, 2019.
- [14] Tianqi Chen and Carlos Guestrin. XGBoost: A scalable tree boosting system. In *Proceedings of the 22nd ACM SIGKDD International Conference on Knowledge Discovery and Data Mining*, KDD '16, pages 785–794, New York, NY, USA, 2016. ACM. URL: <http://doi.acm.org/10.1145/2939672.2939785>, doi: 10.1145/2939672.2939785.
- [15] Carlos A Coello Coello and Margarita Reyes Sierra. A study of the parallelization of a coevolutionary multi-objective evolutionary algorithm. In *Mexican international conference on artificial intelligence*, pages 688–697. Springer, 2004.
- [16] Kalyanmoy Deb, Amrit Pratap, Sameer Agarwal, and TAMT Meyarivan. A fast and elitist multiobjective genetic algorithm: Nsga-ii. *IEEE transactions on evolutionary computation*, 6(2):182–197, 2002.
- [17] M. Ehrgott. *Multicriteria optimization*. Springer Science & Business Media, 2006.
- [18] M. Ehrgott, X. Gandibleux, and A. Przybylski. Exact methods for multi-objective combinatorial optimisation. In *Multiple Criteria Decision Analysis*, pages 817–850. Springer, 2nd edition, 2016.
- [19] Matteo Fischetti, Fred Glover, and Andrea Lodi. The feasibility pump. *Mathematical Programming*, 104:91–104, 2005.
- [20] Md Shamim Hussain, Mohammed J Zaki, and Dharmashankar Subramanian. Global self-attention as a replacement for graph convolution. In *Proceedings of the 28th ACM SIGKDD Conference on Knowledge Discovery and Data Mining*, pages 655–665, 2022.
- [21] Moksh Jain, Sharath Chandra Raparthy, Alex Hernández-García, Jarrid Rector-Brooks, Yoshua Bengio, Santiago Miret, and Emmanuel Bengio. Multi-objective gflownets. In *International Conference on Machine Learning*, pages 14631–14653. PMLR, 2023.
- [22] Thorsten Joachims, Thomas Hofmann, Yisong Yue, and Chun-Nam Yu. Predicting structured objects with support vector machines. *Communications of the ACM*, 52(11):97–104, 2009.
- [23] Gokhan Kirlik and Serpil Sayin. A new algorithm for generating all nondominated solutions of multiobjective discrete optimization problems. *European Journal of Operational Research*, 232(3):479–488, 2014.
- [24] Ryo Kuroiwa and J Christopher Beck. Large neighborhood beam search for domain-independent dynamic programming. In *29th International Conference on Principles and Practice of Constraint Programming (CP 2023)*. Schloss-Dagstuhl-Leibniz Zentrum für Informatik, 2023.
- [25] Chang-Yeong Lee. Representation of switching circuits by binary-decision programs. *The Bell System Technical Journal*, 38(4):985–999, 1959.
- [26] Xi Lin, Zhiyuan Yang, Xiaoyuan Zhang, and Qingfu Zhang. Pareto set learning for expensive multi-objective optimization. *Advances in Neural Information Processing Systems*, 35:19231–19247, 2022.
- [27] Mohsen Nafar and Michael Römer. Using clustering to strengthen decision diagram bounds for discrete optimization. In *Proceedings of the AAAI Conference on Artificial Intelligence*, volume 38, pages 8082–8089, 2024.
- [28] Aviv Navon, Aviv Shamsian, Ethan Fetaya, and Gal Chechik. Learning the pareto front with hypernetworks. In *International Conference on Learning Representations*, 2020.
- [29] Özgür Özpeynirci and Murat Köksalan. An exact algorithm for finding extreme supported nondominated points of multiobjective mixed integer programs. *Management Science*, 56(12):2302–2315, 2010.
- [30] Aritra Pal and Hadi Charkhgard. A feasibility pump and local search based heuristic for bi-objective pure integer linear programming. *INFORMS Journal on Computing*, 31(1):115–133, 2019.
- [31] Aritra Pal and Hadi Charkhgard. Fpbh: A feasibility pump based heuristic for multi-objective mixed integer linear programming. *Computers & Operations Research*, 112:104760, 2019.
- [32] Adam Paszke, Sam Gross, Francisco Massa, Adam Lerer, James Bradbury, Gregory Chanan, Trevor Killeen, Zeming Lin, Natalia Gimelshein, Luca Antiga, et al. Pytorch: An imperative style, high-performance deep learning library. *Advances in neural information processing systems*, 32, 2019.
- [33] Rahul Patel and Elias B Khalil. Leo: Learning efficient orderings for multiobjective binary decision diagrams. In *International Conference on the Integration of Constraint Programming, Artificial Intelligence, and Operations Research*, pages 83–110. Springer, 2024.

-
- [34] Thomas Stidsen, Kim Allan Andersen, and Bernd Dammann. A branch and bound algorithm for a class of biobjective mixed integer programs. *Management Science*, 60(4):1009–1032, 2014.
- [35] Satya Tamby and Daniel Vanderpooten. Enumeration of the nondominated set of multiobjective discrete optimization problems. *INFORMS Journal on Computing*, 33(1):72–85, 2021.
- [36] Fabien Tricoire. Multi-directional local search. *Computers & operations research*, 39(12):3089–3101, 2012.
- [37] Yaoxin Wu, Wen Song, Zhiguang Cao, Jie Zhang, Abhishek Gupta, and Mingyan Lin. Graph learning assisted multi-objective integer programming. In S. Koyejo, S. Mohamed, A. Agarwal, D. Belgrave, K. Cho, and A. Oh, editors, *Advances in Neural Information Processing Systems*, volume 35, pages 17774–17787. Curran Associates, Inc., 2022.
- [38] Manzil Zaheer, Satwik Kottur, Siamak Ravanbakhsh, Barnabas Poczos, Russ R Salakhutdinov, and Alexander J Smola. Deep sets. In I. Guyon, U. Von Luxburg, S. Bengio, H. Wallach, R. Fergus, S. Vishwanathan, and R. Garnett, editors, *Advances in Neural Information Processing Systems*, volume 30. Curran Associates, Inc., 2017.
- [39] Qingfu Zhang and Hui Li. Moea/d: A multiobjective evolutionary algorithm based on decomposition. *IEEE Transactions on evolutionary computation*, 11(6):712–731, 2007.